

Progress towards a high-gain and robust target design for heavy ion fusion

Enrique Henestroza and B. Grant Logan

Citation: [Phys. Plasmas](#) **19**, 072706 (2012); doi: 10.1063/1.4737587

View online: <http://dx.doi.org/10.1063/1.4737587>

View Table of Contents: <http://pop.aip.org/resource/1/PHPAEN/v19/i7>

Published by the [American Institute of Physics](#).

Related Articles

Solid debris collection for radiochemical diagnostics at the National Ignition Facility
[Rev. Sci. Instrum.](#) **83**, 10D904 (2012)

Fast-electron self-collimation in a plasma density gradient
[Phys. Plasmas](#) **19**, 062702 (2012)

Measurements of hohlraum-produced fast ions
[Phys. Plasmas](#) **19**, 042707 (2012)

A polar-drive-ignition design for the National Ignition Facility
[Phys. Plasmas](#) **19**, 056308 (2012)

Multiple spherically converging shock waves in liquid deuterium
[Phys. Plasmas](#) **18**, 092706 (2011)

Additional information on Phys. Plasmas

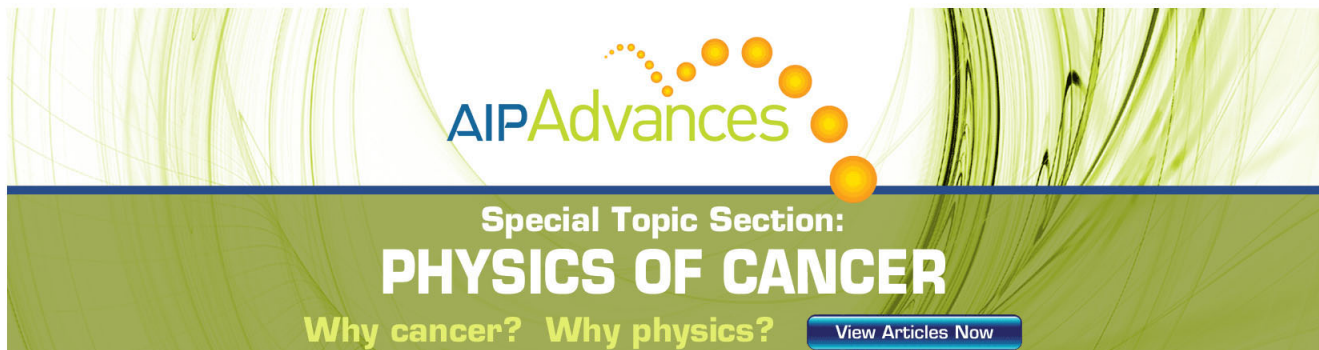
Journal Homepage: <http://pop.aip.org/>

Journal Information: http://pop.aip.org/about/about_the_journal

Top downloads: http://pop.aip.org/features/most_downloaded

Information for Authors: <http://pop.aip.org/authors>

ADVERTISEMENT



AIPAdvances

Special Topic Section:
PHYSICS OF CANCER

Why cancer? Why physics?

[View Articles Now](#)

Progress towards a high-gain and robust target design for heavy ion fusion

Enrique Henestroza and B. Grant Logan

Lawrence Berkeley National Laboratory, Berkeley, California 94720, USA

(Received 16 April 2012; accepted 11 June 2012; published online 19 July 2012)

Recently [E. Henestroza *et al.*, Phys. Plasmas **18**, 032702 (2011)], a new inertial-fusion target configuration, the X-target, using one-sided axial illumination has been explored. This class of target uses annular and solid-profile heavy ion beams to compress and ignite deuterium-tritium (DT) fuel that fills the interior of metal cases that have side-view cross sections in the shape of an "X." X-targets using all-DT-filled metal cases imploded by three annular ion beams resulted in fuel densities of $\sim 50 \text{ g/cm}^3$ at peak compression, and fusion gains of ~ 50 , comparable to heavy ion driven hohlraum targets [D. A. Callahan-Miller and M. Tabak, Phys. Plasmas **7**, 2083 (2000)]. This paper discusses updated X-target configurations that incorporate inside the case a propellant (plastic) and a pusher (aluminum) surrounding the DT fuel. The updated configurations are capable of assembling higher fuel areal densities $\sim 2 \text{ g/cm}^2$ using two annular beams to implode the target to peak DT densities $\sim 100 \text{ g/cm}^3$, followed by a fast-ignition solid ion beam which heats the high-density fuel to thermonuclear temperatures in $\sim 200 \text{ ps}$ to start the burn propagation, obtaining gains of ~ 300 . These targets have been modeled using the radiation-hydrodynamics code HYDRA [M. M. Marinak *et al.*, Phys. Plasmas **8**, 2275 (2001)] in two- and three- dimensions to study the properties of the implosion as well as the ignition and burn propagation phases. At typical Eulerian mesh resolutions of a few microns, the aluminum-DT interface shows negligible Rayleigh–Taylor (RT) and Richtmyer–Meshkov instability growth; also, the shear flow of the DT fuel as it slides along the metal X-target walls, which drives the RT and Kelvin Helmholtz instabilities, does not have a major effect on the burning rate. An analytic estimate of the RT instability process at the Al-DT interface shows that the aluminum spikes generated during the pusher deceleration phase would not reach the ignition zone in time to affect the burning process. Also, preliminary HYDRA calculations, using a higher resolution mesh to study the shear flow of the DT fuel along the X-target walls, indicate that metal-mixed fuel produced near the walls would not be transferred to the DT ignition zone (at maximum ρR) located at the vertex of the X-target. © 2012 American Institute of Physics. [<http://dx.doi.org/10.1063/1.4737587>]

I. INTRODUCTION

In a previous paper,¹ a new inertial-fusion target configuration, the X-target, using one-sided axial illumination has been explored. This class of target uses annular and solid-profile heavy ion beams to compress and ignite deuterium-tritium (DT) fuel that fills the interior of metal cases that have side-view cross sections in the shape of an "X." The HYDRA (Ref. 2) radiation-hydrodynamics code was used in axisymmetric 2D to find target configurations to produce quasi-spherical compression of the fuel toward the X-vertex on axis by controlling the geometry of the case, and the successive timing, power, and radii of nested annuli of ion beams. As reported,¹ X-targets consisting of all-DT-filled metal cases imploded by three annular ion beams (Fig. 1) resulted in peak fuel densities of $\sim 50 \text{ g/cm}^3$ at peak compression, and fusion gains of ~ 50 , comparable to heavy ion driven hohlraum targets.³

In this paper, we find much higher target gains of 300 in X-target configurations by incorporating inside the case a propellant (plastic) and a pusher (aluminum) surrounding the DT fuel. These configurations are capable of assembling higher fuel areal densities $\sim 2 \text{ g/cm}^2$ using two annular beams to implode the target. As a result, only 2 MJ of compression beam energy is required with two compression pulses, instead

of 3 MJ with three compression pulses as in the previous all-DT version.¹ Because of the higher fuel ρR , much higher fuel burnup fractions (0.2) and fusion yields (1.5 GJ) are obtained, so that with 3 MJ of fast-ignition beam energy, we obtain gains of ~ 300 . The inclusion of a propellant, and a pusher which later in time becomes a higher-pressure propellant (as an "exploding pusher") improves implosion compression efficiency. This is achieved by improving the coupling efficiency of the ion beam energy, particularly from the second compression beam to the aluminum pusher, which can transfer more of its kinetic energy to the fuel. Furthermore, the outer case improves the first compression beam's coupling by acting as a radial tamper. The numerical simulations include hydro effects of the beams penetrating and heating all the components of the X-target. The metal case is important for tamping; and expansion of the case can be tailored to improve the quasi-spherical symmetry of the initial fuel compression. The implosion phase of the X-target does not change appreciably when radiation transport is turned off in the calculations; this shows that radiation drive is unimportant to the fuel compression, compared to hydro pressure.

The six-fold increase in gain of the new X-target is obtained via an increase by a factor of two in the implosion velocity of the DT fuel, thus, producing a higher stagnation density as well as a higher areal density at the ignition zone.

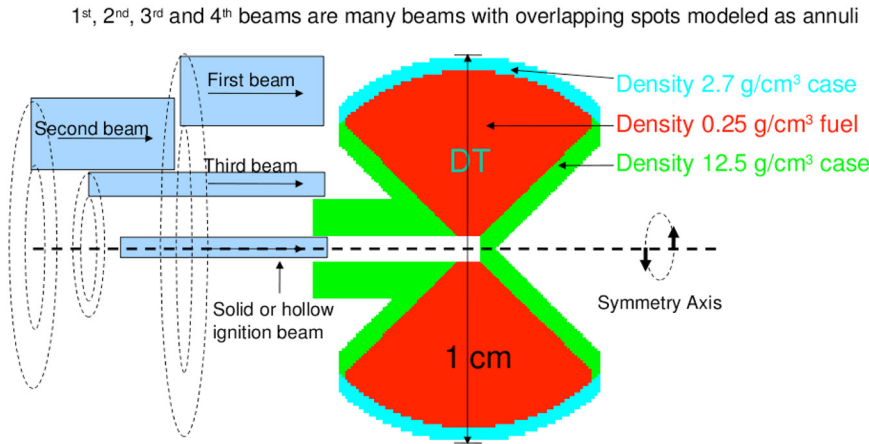


FIG. 1. Low gain version of the X-target.

However, this higher gain comes at a potential cost in increased complexity of the X-target configuration; and the increase in the implosion velocity could make this new target more susceptible to hydrodynamic instabilities. Since the fuel is a solid sector of a sphere, the X-target is not subject to problems of fuel-layer integrity as is the case in the implosion of thin spherical fuel shells; the main concern for the X-target is the amount of high-Z atomic mixing produced at the ignition zone, which, if large enough, could cool down the fuel during the ignition process and prevent the propagation of the fusion burn. We have identified two mechanisms as possible sources of high-Z mixing: the Rayleigh–Taylor (RT) instability taking place during the deceleration phase at the aluminum-DT (pusher-fuel) interface, and the RT/Kelvin Helmholtz (KH) instability taking place when the DT fuel compresses and slides along the high-Z side walls of the X-target. We have found that for relatively low implosion velocities (~ 60 km/s), low stagnation fuel densities ~ 100 g/cm³, and quasi-spherical fuel convergence ratios of ~ 7 , the aluminum spikes generated during the pusher deceleration phase at the pusher-fuel interface do not reach the ignition zone in time to affect the burning process. We have also found, by tracing the fluid motion, that the RT/KH vortices generated on the X-target walls are pushed in the direction of the wall motion, away from the axial mid-plane of the target, and the residual debris that enters the target vertex

is removed by a DT jet that arrives at this location just before the bulk of the fuel compresses to a high density. A third mechanism of potential high-Z mixing is due to jets generated by high pressure gradients produced by the ion beam Bragg-peak stopping in the rear side-case wall; but the X-target architecture allows for design adjustments where these jets can be avoided or directed away from the ignition zone.

The remainder of the paper is organized as follows. In Sec. II, we introduce the new configuration of the X-target and describe the results of the HYDRA simulations. In Sec. III, we analyze the interface stability of the X-target, including the dynamics of the pusher-fuel interface and the shear flow of the DT fuel along the X-target walls. In Sec. IV, we summarize the distinctive attributes of the high-gain X-target configuration and conclude with plans for future work.

II. RADIATION HYDRODYNAMIC SIMULATIONS OF THE HIGH-GAIN X-TARGET

The axial cross section of the new layout is shown in Figure 2, and a 3D rendering in Figure 3). This layout allows for the optimization of the pressure profile produced by the deposition of the ion beam energy, as well as the transfer of kinetic energy to the fuel by the pusher; furthermore, the case is now used as a radial tamper. Fig. 2 also shows the location of the two annuli of heavy ion beams used for

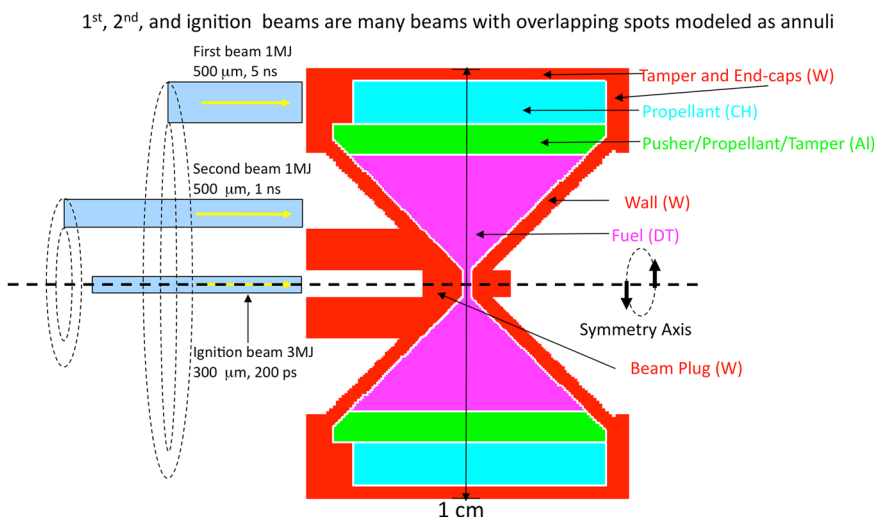


FIG. 2. High gain version of the X-target.

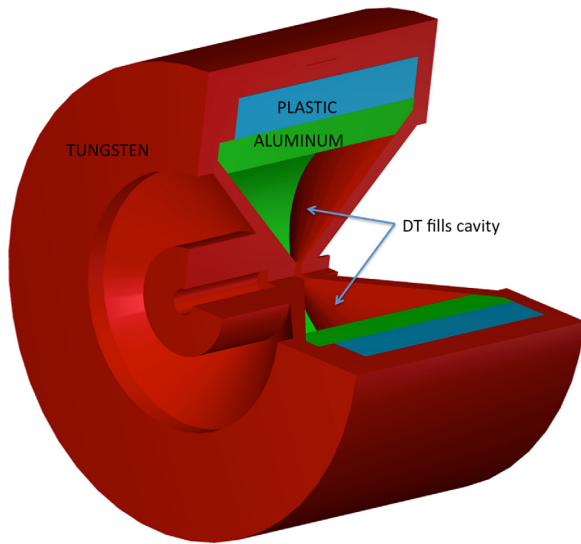


FIG. 3. 3D rendering of the high-gain version of the X-target. Color code as in Fig. 2. The DT fuel is not included.

compression, as well as the solid central beam used for ignition. The implosion requires two 1 MJ ion beam annuli; the pulse lengths are 5-ns and 1-ns Gaussian FWHM, with the second implosion beam injected ~ 120 ns after the first; the width of both annuli are $500 \mu\text{m}$ Gaussian FWHM. The ignition beam is a 3 MJ solid ion beam of 100 ps Gaussian FWHM pulse length (total width of 400 ps), injected at the time of maximum compression (~ 136 ns); the beam size is $300 \mu\text{m}$ Gaussian FWHM. The overall dimension of the target is 1 cm in diameter.

The implosion phase of the X-target is described in Figure 4 by three snapshots taken at the times of peak-power of the first (Fig. 4(a)) and second ion beams (Fig. 4(b)), and at time of maximum compression (Fig. 4(c)) which is the end of the implosion phase. Figure 4(d) shows the material distribution at this time of maximum compression (beginning of the ignition phase) when the ignition beam is injected; the volume and areal fuel densities reach values of $\sim 120 \text{ g/cm}^3$ and $\sim 2 \text{ g/cm}^2$, respectively. The numerical simulations include full radiation hydrodynamic effects of the

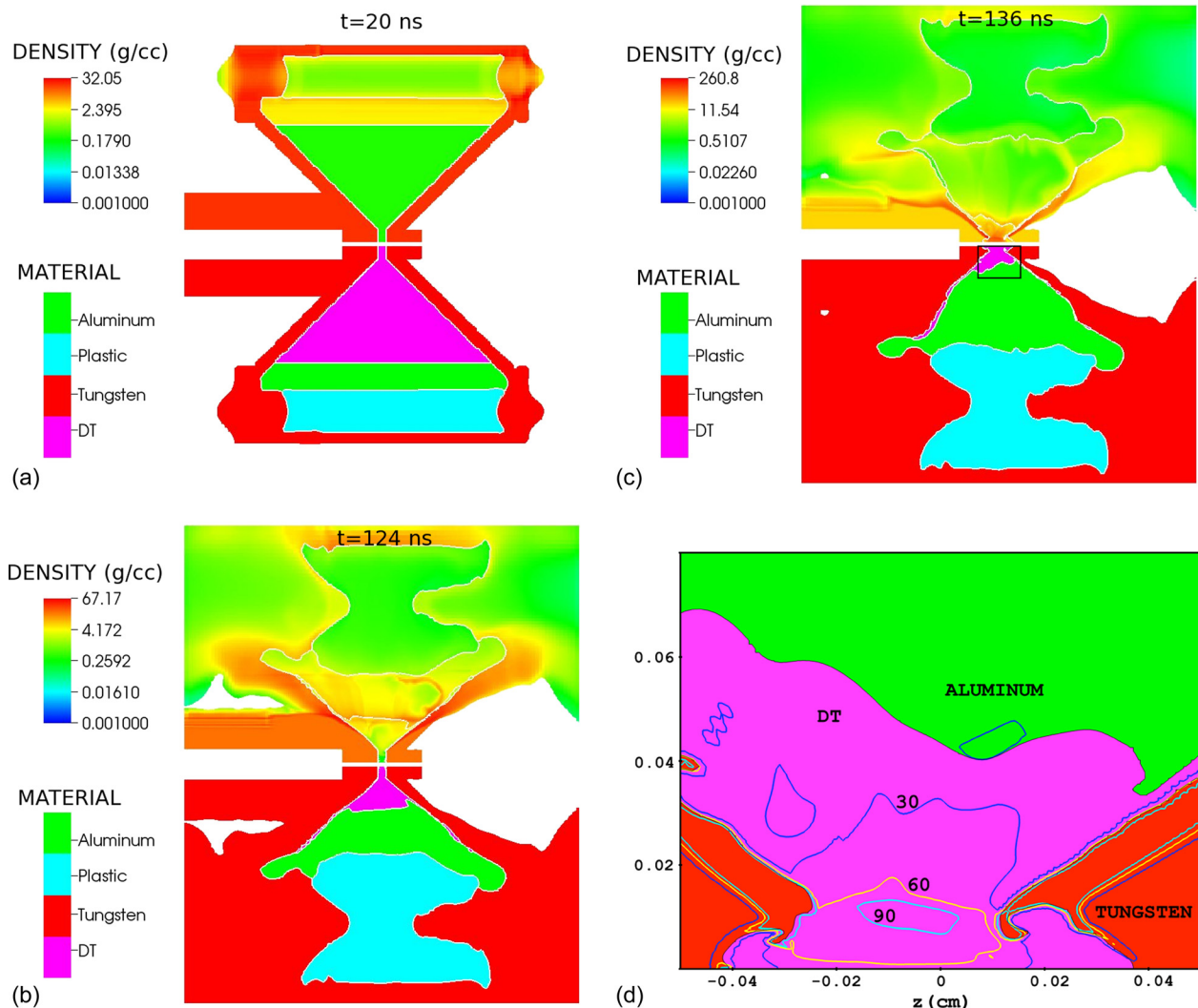


FIG. 4. Snapshots of implosion phase showing the density (g/cm^3) distribution (top of each figure) and material distribution (bottom of each figure) at the time when (a) the first and (b) the second implosion beams are passing through the target, and (c) at time of maximum compression just before the ignition beam is turned on. In (d), the material distribution and three density contours (30, 60, and 90 g/cm^3) are shown in the region marked with the black square in (c).

beams penetrating and heating all the components of the X-target, assuming axisymmetric target and annular and solid beams.

The ion-beam energy deposition is calculated in HYDRA by tracing the ion beam along a rectilinear trajectory and computing the absorbed energy in each mesh cell using a classical formula for energy loss in partially ionized plasmas. This generalized Bethe formula⁴ includes contributions for both bound and free electrons, and uses the Betz formula for the effective charge state of the ion.

The HYDRA calculations also show that the implosion (and ignition) dynamics is minimally affected by a change of the ion species as long as the ranges are the same; thus, we could use, e.g., 20 GeV rubidium or 90 GeV uranium ion beams.

The implosion dynamics is modified by 3D effects produced by the fact that the annular beams may be composed of individual solid beams located in a ring pattern, which breaks the assumption of rotational symmetry; these effects were studied for the case of a periodic layout of 20 beams along the azimuth; the 3D simulation was performed taking an 18° wedge of the X-target containing a single round solid beam and applying periodic boundary conditions. The results show a small effect on the final densities, effects that may be minimized by a further optimization of the beam parameters.

The ignition phase was modeled by full radiation hydrodynamics calculations including thermonuclear burn using HYDRA on an Eulerian mesh; radiation transport was modeled with multi-group (50 energy groups) radiation diffusion or implicit Monte Carlo photonics, and transport and deposition of energetic charged particles produced by thermonuclear reactions were included. Figures 5 and 6 show the pressure and temperature distribution at the time of ignition-beam peak power and at the time of peak fusion power. We obtain fusion yields of ~ 1.5 GJ for a gain of ~ 300 .

Finally, during the implosion phase, and at typical Eulerian mesh resolutions of a few microns, as seen in Fig. 4, the aluminum-DT interface shows negligible RT and Richtmyer–Meshkov (RM) instability growth. The shear

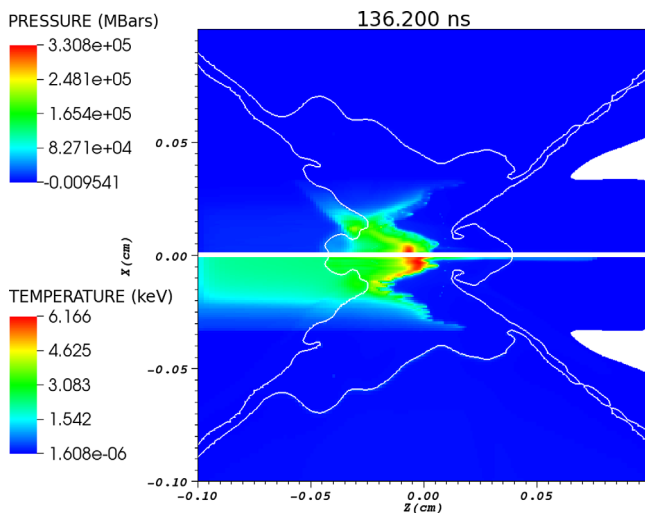


FIG. 5. Pressure (Megabars) and temperature (keV) at ignition-beam peak power (200 ps after end of implosion phase).

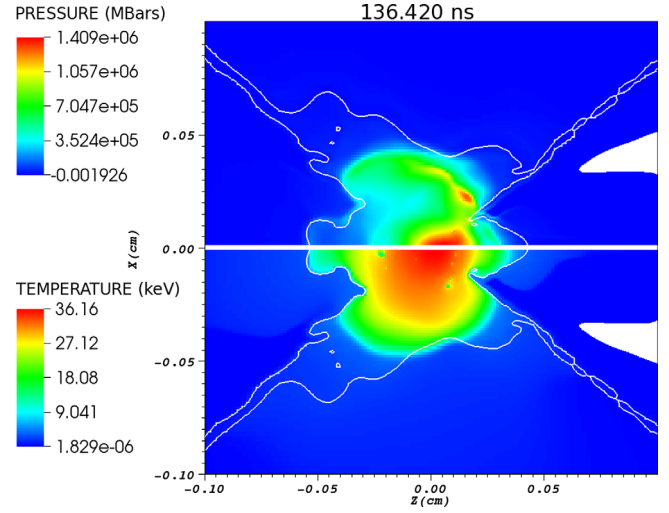


FIG. 6. Pressure (Megabars) and temperature (keV) at peak fusion power (420 ps after end of implosion phase).

flow of the DT fuel as it slides along the metal X-target walls drives the RT and KH instabilities, which are seen to grow (notice the white interface structure shown in Figs. 5 and 6) but do not have a major effect on the burning rate.

The next section presents a preliminary analysis of the interface stability of the X-target, including the dynamics of the pusher-fuel interface and the shear flow of the DT fuel along the X-target walls, as well as on the effects of high-Z material mix on burn propagation.

III. PRELIMINARY ANALYSIS OF THE INTERFACE STABILITY OF THE X-TARGET

A. RT and RM instability at the pusher-fuel interface

At typical Eulerian mesh resolutions of a few microns, the aluminum-DT interface shows negligible RT and RM instability growth and these modes do not produce a major effect on the burning rate. Therefore, the effect of these interface instabilities have to be estimated using turbulent atomic mix models.

The implosion dynamics of the X-target shows that the deceleration phase of the pusher-fuel interface, which breeds

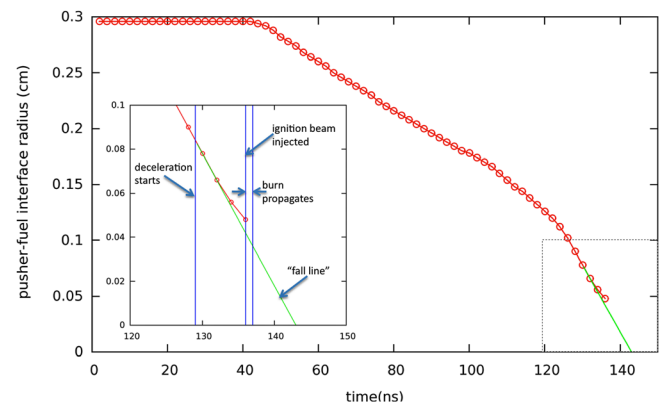


FIG. 7. Pusher-fuel-interface trajectory for the high-gain X-target configuration. The inset shows the relevant timings of the implosion and fuel burn dynamics.

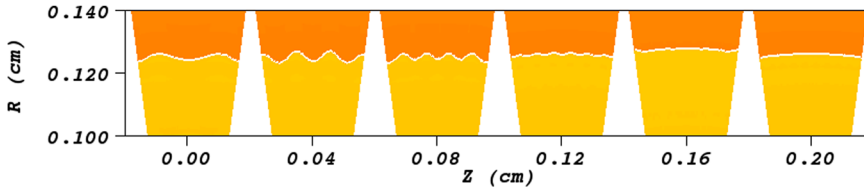


FIG. 8. Snapshots, at time of injection of the second beam, showing Richtmyer–Meshkov 2D-single-mode calculations at the pusher-fuel interface for modes $\ell = 36, 72, 108, 144, 180, 216$, and initial perturbations with $1\ \mu\text{m}$ amplitude, using a surrogate configuration that mimics the implosion dynamics of the X-target.

the RT instability, starts at 129 ns and lasts for 7 ns, at which time the ignition beam is injected. The average interface deceleration is $a \sim 4.3 \times 10^{14}\text{ cm/s}^2$ at a radius of 0.0840 cm, with the speed decreasing from $v \sim 6 \times 10^6\text{ cm/s}$ to $3 \times 10^6\text{ cm/s}$, which translates into a free-fall time of 14 ns. As shown in Fig. 7, the spikes generated by the RT instability would not reach the ignition region ($r \sim 0.0250\text{ cm}$) even if they were to follow the “fall line.”

The following analytic estimates of RT/RM instability growth follow closely the analysis described in the book of Atzeni and Meyer-ter-Vehn.⁵

The growth rates and e-folding times can be estimated from the classical formulas. The Atwood number is found to be almost constant and equal to 0.2 during that interval; therefore, the classic e-folding time in seconds for perturbations of wavenumber k is $\sim 1 \times 10^{-7}/\sqrt{k}$ with k in cm^{-1} . Thus, for perturbations of (spherical) mode number $\ell = 36$ at $R = 0.06\text{ cm}$, we have $k = 600\text{ cm}^{-1}$, which produces an e-folding time of $\sim 4\text{ ns}$. For perturbations of mode number $\ell = 216$, we have $k = 3600\text{ cm}^{-1}$, which produces an e-folding time of $\sim 1.7\text{ ns}$. These estimates show that only high order modes >36 could grow enough to perturb the dynamics at the ignition zone.

We can also estimate the penetration depth of the instability arising from random perturbations. The time evolution of the width of the turbulent mixing layer due to RT/RM instability can be qualitatively described by dimensional arguments.⁵ The width of the mixing layer at the interface is proportional to $A*a*t^2$, where A is the Atwood number, a is the interface acceleration, and t is the time during which the instability persists; the factor of proportionality is around 4%–7% as obtained from fits to experimental results. From the values already provided, we estimate a penetration depth of $5\ \mu\text{m}$.

Therefore, this RT/RM instability analysis at the pusher-fuel interface estimates that the aluminum spikes generated during the pusher deceleration phase would not reach the ignition zone in time to affect the burning process. However, more work is needed with higher resolution over the entire X-target, to be sure no aluminum metal jets (sometimes observed near the ignition zone) are created by beam Bragg peaks hitting the walls in the outer case. Our analysis, while encouraging, needs to be confirmed by experiments.

In a personal communication in Ref. 10, we were informed that a k-L turbulence model⁶ calculation of an equivalent X-target design shows that the pusher-fuel interface does not generate enough high-Z mix to affect the ignition process.

Preliminary numerical studies of the effect of Richtmyer–Meshkov instability on the pusher-fuel interface were performed using 2D-single-mode HYDRA calcula-

tions. A surrogate configuration consisting of a 15° polar wedge of a sphere that mimics the implosion dynamics of the X-target from the initial time to the time just before the injection of the second implosion beam, allows for calculations using a Lagrangian mesh that can resolve Legendre modes up to $\lambda = 216$; but this configuration (a polar wedge of a sphere) is not a good model for the X-target fluid dynamics at later times. Figure 8 depicts snapshots at the end of the simulation showing small growth factors (<50) for initial perturbations of amplitude $1\ \mu\text{m}$. Further calculations are in progress to complete the numerical analysis.

B. RT and KH instability at DT-wall interface

It is well known⁷ that the shear flow of the DT fuel along the X-target walls is always KH unstable, i.e., the shear flow develops vortices flowing along the walls; furthermore, since the low density fuel is compressing the high density wall, the flow is also RT unstable.

As already mentioned above, at typical Eulerian mesh resolutions of a few microns, the RT and KH instabilities driven by the shear flow of the DT fuel as it slides along the metal X-target side walls, are seen to grow in our HYDRA simulations but do not have a major effect on the burning rate. Preliminary HYDRA calculations, using a higher resolution mesh to study the shear flow of the DT fuel along the X-target walls, indicate that metal-mixed fuel produced near the walls would not be transferred to the DT ignition zone (at maximum ρR) located at the vertex of the X-target.

Figures 9 and 10 show trajectories obtained by tracing fluid elements along the wall region during implosion of the X-target; they show the particles convecting away from the ignition zone. These preliminary calculations also show that

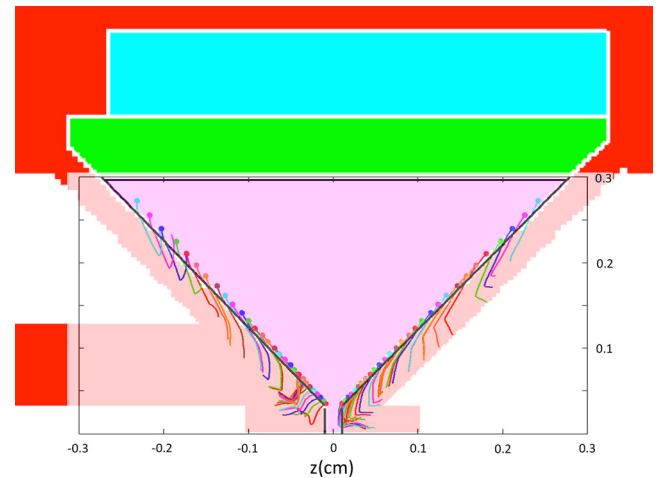


FIG. 9. Fluid element traces along the X-target wall region during implosion. The dots indicate the starting points of the trajectories.

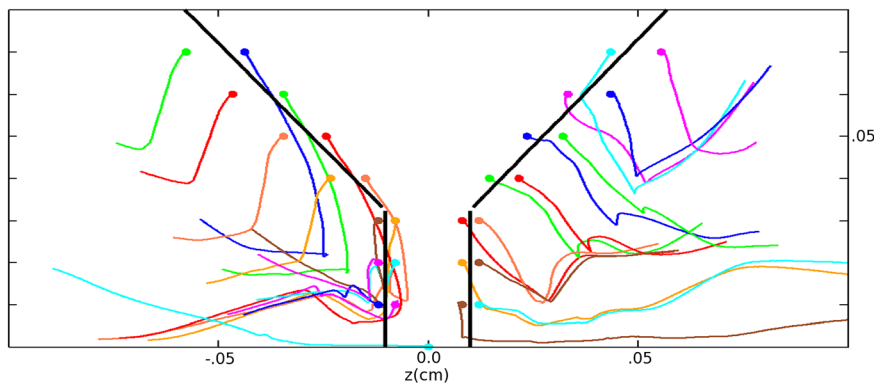


FIG. 10. Fluid element traces along the X-target wall region, and near the ignition zone, during implosion. The dots indicate the starting points of the trajectories.

the high-Z material appearing near the ignition zone consists of large pieces of metal broken away from the walls or from the pusher; these “chunks” of high-Z material are not harmful to the burn propagation since the fuel “burns around” them.

Further hydrodynamic calculations using finer resolutions, complemented with turbulent mix models are required to ascertain the stability of the X-target design.

IV. SUMMARY AND CONCLUSIONS

Based on the original X-target concept for the production of quasi-spherical compression and fast-ignition using heavy-ion beams, we have designed a new target which is composed of a solid core of DT (fuel) enclosed in an aluminum shell (pusher) which is also enclosed in a plastic shell (propellant); these three components are surrounded by a tungsten case (tamper) in an X-configuration. Enough fuel is assembled to an areal density of $\rho R \sim 2 \text{ g/cm}^2$ and density of $\rho \sim 120 \text{ g/cm}^3$ to be ignited by an ion beam and start the burn propagation to the lower density fuel. Two 1 MJ, 20 GeV annular rubidium (or 90 GeV uranium) beams provide the implosion energy; the first phase of the implosion starts when the first ion beam deposits its energy in the propellant; after $\sim 120 \text{ ns}$, and before the aluminum pusher starts to decelerate, the second ion beam is made to deposit its energy in the pusher so as to start the second phase of the implosion. At maximum compression, a 3 MJ, 20 GeV solid rubidium beam deposits enough energy at the high fuel density region to ignite the fuel and start the burn propagation. The fusion yield is $\sim 1.5 \text{ GJ}$ for a gain of 300. The design parameters are based on two-dimensional calculations using the radiation-hydrodynamics code HYDRA. 3D effects produced by the fact that the annular beams may be composed of individual solid beams located in a ring pattern, which breaks the assumption of rotational symmetry, are shown to have a minimal effect on the implosion phase. Based on analytic estimates and hydrodynamics simulations using Eulerian mesh resolutions of a few microns, Rayleigh-Taylor instability mix at the pusher-fuel interface and the Kelvin-Helmholtz hydrodynamic instability excited by the fuel sliding along the walls of the X-target are found to have a minor influence on ignition and subsequent fuel burn-up.

The very high ion kinetic energies used by, and the high gains afforded by the X-target, motivate the consideration of high gradient (lower efficiency) RF linacs as well as induc-

tion linacs as drivers; more study of accelerator options for the X-target is needed. Calculations to be reported elsewhere, taking into account the transverse and parallel emittance growth of the heavy ion beams, show that such ion beams in linacs should have sufficient brightness to drift-compress to 200 ps and to focus into plasma-neutralized chambers to a spot radius less than $300 \mu\text{m}$, as required to fast-ignite the compressed DT near the vertex of the X-target. Scaled compression focusing physics experiments related to the X-target are planned within a couple of years using the NDCX-II accelerator,⁸ now being commissioned. In Ref. 9, an experimental RF-accelerator driver for Heavy Ion Fast Ignition is described; the beam parameters are comparable to those required to drive the X-target.

The X-target’s construction of an extruded metal case filled with hard-frozen-DT (no beta-layering needed) should be conducive to low cost, low precision, mass manufacture. The rigidity of the filled X-target case tolerating extremely high gyroscopic spin frequencies, and tolerance for residual offset and tilt errors as seen in preliminary calculations, should facilitate target injection into hot gas chambers and adequate alignment of its axis with the ion-beam annuli. In addition to these qualities, the X-target’s robustness to the amount of high-Z mixing from interface instabilities (to be validated by future experiments) makes the X-target’s potential for a high-gain and robust design for heavy ion fusion more likely to be realized.

Near-term work is focused on analytic and numerical hydro-stability (mix due to RT and KH) studies of the fuel implosion using turbulent atomic mix models. Also work on mitigation methods to control the high-Z mix problem is planned; there are a number of side-wall-mix mitigating strategies that have yet to be investigated to explore how much higher X-target gains in 2- and 3D might be optimized towards the 1D potential gain of 1000. Since there are so many such optimization opportunities, we would welcome a wider collaboration to make progress faster. Finally, we would like to emphasize the fact that RT-RM-KH surrogate data from experiments would be very helpful to confirm the simulations.

ACKNOWLEDGMENTS

B. G. Logan gratefully acknowledges useful discussions with Robert Tipton on his results of numerical simulations of

the X-target. We are very grateful to the anonymous reviewer for comments that improved the quality of this manuscript. This work was performed under the support of the U.S. Department of Energy by the Lawrence Berkeley National Laboratory under Contract No. DE-AC02-05CH11231.

¹E. Henestroza, B. G. Logan, and L. J. Perkins, *Phys. Plasmas* **18**, 032702 (2011).

²M. M. Marinak, G. D. Kerbel, N. A. Gentile, O. Jones, D. Munro, S. Pol-laine, T. R. Dittrich, and S. W. Haan, *Phys. Plasmas* **8**, 2275 (2001).

³D. A. Callahan-Miller and M. Tabak, *Phys. Plasmas* **7**, 2083 (2000).

⁴B. G. Logan, L. J. Perkins, and J. J. Barnard, *Phys. Plasmas* **15**, 072701 (2008).

⁵S. Atzeni and J. Meyer-ter-Vehn, *The Physics of Inertial Fusion*, International Series of Monographs on Physics No. 125 (Oxford Science, 2004).

⁶G. Dimonte and R. Tipton, *Phys. Fluids* **18**, 085101 (2006).

⁷S. Chandrasekhar, *Hydrodynamics and Hydromagnetic Stability* (Dover, New York, 1981).

⁸A. Friedman, J. J. Barnard, R. H. Cohen, D. P. Grote, S. M. Lund, W. M. Sharp, A. Faltens, E. Henestroza, J.-Y. Jung, J. W. Kwan, E. P. Lee, M. A. Leitner, B. G. Logan, J.-L. Vay, W. L. Waldron, R. C. Davidson, M. Dorf, E. P. Gilson, and I. D. Kaganovich, *Phys. Plasmas* **17**, 056704 (2010).

⁹B. Y. Sharkov, N. N. Alexeev, M. M. Basko, M. D. Churazov, D. G. Kosh-karev, S. A. Medin, Y. N. Orlov, and V. M. Suslin, *Nucl. Fusion* **45**, S291 (2005).

¹⁰R. Tipton, personal communication (August 2011).